ACS APPLIED MATERIALS & INTERFACES

Research Article

www.acsami.org

Chemiresistive Sensing Behavior of SnO_2 (*n*)–Cu_2O (*p*) Core–Shell Nanowires

Jae-Hun Kim,[†] Akash Katoch,[†] Soo-Hyun Kim,*[,‡] and Sang Sub Kim*[,†]

[†]Department of Materials Science and Engineering, Inha University, Incheon 402-751, Republic of Korea

[‡]School of Materials Science and Engineering, Yeungnam University, Gyeongsangbuk-do 712-749, Republic of Korea

Supporting Information

ABSTRACT: We report the synthesis of SnO_2–Cu_2O *n*–*p* core–shell nanowires (C–S NWs) and their use as chemiresistive sensors for detecting trace amounts of gas. The *n*–*p* C–S NWs were synthesized by a two-step process, in which the core SnO_2 nanowires were prepared by the vapor growth technique and subsequently the Cu_2O shell layers were deposited by atomic layer deposition. A systematic investigation of the sensing capabilities of the *n*–*p* C–S NWs, particularly as a function of shell thickness, revealed the underlying sensing mechanism. The radial modulation of the hole-accumulation layer is intensified under shells thinner than the Debye length. On the other hand, the contribution of volume fraction to resistance modulation is weakened. By the combination of these two effects, an optimal sensing performance for reducing gases is obtained for a critical *p*-shell thickness. In contrast, the formation of *p*-shell layers deteriorates the NO_2-sensing performance by blocking the expansion of the hole-accumulation layer due to the presence of *p*–*n* heterointerface.

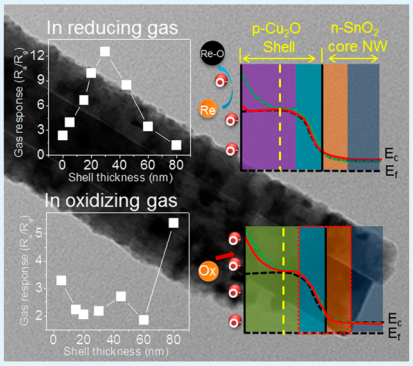

KEYWORDS: *SnO_2–Cu_2O, core–shell, nanowires, p–n junction, sensing mechanism*

1. INTRODUCTION

Detection of trace amounts of hazardous chemical species is essential to prevent catastrophic chemical disasters in modern industries. Over the past few decades, a huge number of sensor materials have been developed to this end. The key parameters considered in the field of chemiresistive sensors are the degree of gas-response, the response and recovery times, and selective detectability.[1−3] It is required that gas-responses are high enough to detect extremely low concentrations, which is essential to the use of chemiresistive sensors to analyze exhaled breath for disease diagnosis.[4,5]

Oxide nanowires (NWs) have gained increasing attention as promising chemiresistive sensor materials owing to their advantageous properties, including a large surface area, single-crystalline quality, and high intrinsic modulation of electrical transport due to the Debye dimension.[6−8] Despite the outstanding sensing abilities of single-oxide NWs, their actual application in commercial sensors is unrealistic due to aspects of their fabrication and reliability.[9] To circumvent such drawbacks involved in single-oxide NW sensors, multiply networked oxide NWs have been synthesized and proved to be excellent sensor platforms.[10,11]

Various attempts have been made to improve further the sensing performance of multiply networked oxide NWs.[12−21] The application of core–shell (C–S) heterostructures has been found to be beneficial for enhancing sensing capabilities of nanomaterials.[19−23] In such structures, a heterojunction is created at the core–shell interface and can enhance the sensing capabilities, provided the shell thickness is equivalent to the Debye length of the shell material. Fe_2O_3/ZnO heteronanostructures exhibited a dramatic improvement in ethanol sensing characteristics compared to the pure Fe_2O_3 nanorods.[19] On the basis of the space-charge layer model, such enhanced sensing properties were attributed to the small thickness of the ZnO shell. In addition, the ZnO/ZnS core/shell nanorods showed improved sensing properties in comparison to pure ZnS nanotubes.[20] Very recently, the sensing mechanism of SnO_2–ZnO C–S NWs, in which *n*-type ZnO shells were formed on an *n*-type SnO_2 core, was systematically investigated.[21] Both the radial modulation of the electron-depleted shell layer and the electric-field smearing effect were found to govern their sensing mechanism, which can be applied to other *n*–*n* material combinations.

As far as the authors know, an investigation on the sensing behaviors of *n*–*p* C–S NWs has not been done yet. In conjunction with previous results regarding *n*–*n* C–S NWs,[21] a more comprehensive sensing mechanism can be established for any combination of C–S NWs. Herein, we report the novel synthesis of *p*-type shells on an *n*-type core NW, namely *n*–*p* SnO_2–Cu_2O C–S NWs. The sensing performances of the *n*–*p* C–S NWs were tested as a function of the *p*-type Cu_2O shell thickness in terms of representative oxidizing and reducing gases, and the underlying sensing mechanism has been proposed.

Received: April 14, 2015
Accepted: June 29, 2015
Published: June 29, 2015

DOI: 10.1021/acsami.5b03224
ACS Appl. Mater. Interfaces 2015, 7, 15351−15358

2. EXPERIMENTAL SECTION

Preparation of SnO_2−Cu_2O C−S NWs. The sensors were fabricated with SnO_2−Cu_2O *n*−*p* C−S NWs by three steps. First, a patterned interdigital electrode (PIE) was deposited on a SiO_2-grown Si (100) substrate by using conventional photolithography. The PIE was an Au (3 nm)/Pt (200 nm)/Ti (50 nm) trilayer, which were sequentially deposited by sputtering from the corresponding metal targets. The Au top layer was the catalytic layer for the selective growth of SnO_2 NWs; the Pt layer allowed electrical current passage in the fabricated sensor; the Ti layer enhanced the adhesion between the Pt layer and the substrate. In the second step, SnO_2 NWs were grown on PIE by evaporating a Sn source in a tube furnace as per the well-known vapor growth method.[24] SnO_2 NWs grown on adjacent PIE pads became entangled, creating a network. The procedure is described in detail in our earlier reports.[25,26] Lastly, Cu_2O shell layers were deposited on the networked SnO_2 NWs by atomic layer deposition (ALD) using a traveling-wave-type ALD reactor (Lucida D100, NCD Technology, Korea), which is a particularly effective method for synthesizing a uniform, conformal layer on irregularly shaped substrates. Bis(1-dimethylamino-2-methyl-2-butoxy)copper ($C_{14}H_{32}N_2O_2Cu$) and water vapor (H_2O) were used as a precursor and a reactant, respectively. The Cu precursor was vaporized in a bubbler at 80 °C and carried into the process chamber by N_2 gas at a flow rate of 200 sccm. The line temperature was maintained at 120 °C to prevent condensation of the Cu precursor during delivery. Water vapor prepared in a canister kept at 100 °C was provided into the chamber without a carrier gas. The temperature and pressure of the reactor were maintained at 140 °C and ∼1 Torr, respectively. The basic pulsing conditions were set as follows: precursor pulsing for 5 s, reactant pulsing for 5 s, and purging for 10 s, which were found to be enough to guarantee a self-limited growth of the Cu_2O film. The sequence of precursor pulsing, purging, reactant pulsing, and purging occurs in each ALD cycle. In this way, SnO_2−Cu_2O C−S NWs with uniform shell thicknesses were synthesized. By changing the number of ALD cycles, the Cu_2O shell thicknesses were successfully controlled to be in the range 5−80 nm. The fabrication sequence of the sensors is shown in Figure 1.

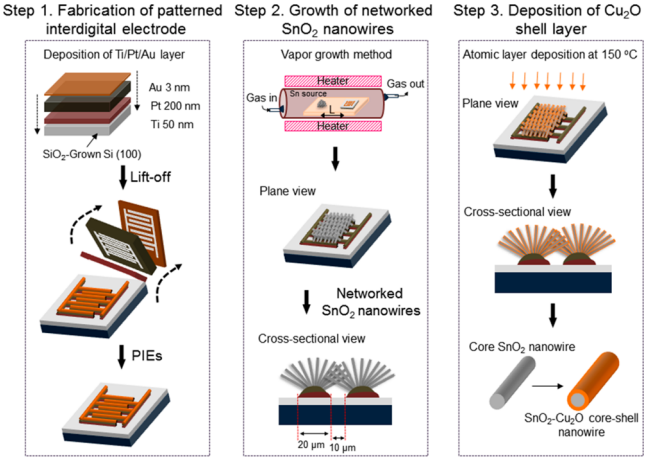

Figure 1. Schematic of the fabrication sequence of sensors based on SnO_2−Cu_2O *n*−*p* C−S NWs.

Characterizations. The overall morphology of the synthesized C−S NWs was observed by field emission scanning electron microscopy (FE-SEM). The detailed crystal structure, microstructure, and chemical composition were examined using transmission electron microscopy (TEM) and energy-dispersive X-ray spectroscopy (EDS). X-ray diffraction (XRD) was used to identify the phase of the C−S NWs. For TEM analysis, the samples were prepared as follows. First, the synthesized C−S NWs were dispersed in ethanol and subsequently sonicated in an ultrasonic bath (BRANSON, 5510EDTH) for 10 min in order to achieve uniform dispersion. The prepared C−S NWs solution was then dropped over an Ni grid and dried under vacuum conditions.

Sensing Measurement. The sensing performances of the C−S NW sensors were investigated as a function of shell thickness using the reducing gases, toluene (C_7H_8) and benzene (C_6H_6), and an oxidizing gas, NO_2. The sensing measurements were carried out at an optimal operating temperature of 300 °C, determined from preliminary experiments. The experimental procedures are described in detail in our earlier report.[13] The gas responses (R) of SnO_2−Cu_2O C−S NWs were evaluated using the equation $R = R_g/R_a$ (or R_a/R_g), where R_a and R_g are the resistances in the absence and presence of an analyte gas, respectively, for an oxidizing gas (a reducing gas).

3. RESULTS AND DISCUSSION

As Figure 1 demonstrates, by having a suitable spacing in the PIE, well-networked SnO_2 NWs can be attained. FE-SEM images (in-plane-view and cross-sectional view, not presented here) showed the entangled SnO_2 NWs that act as a chemiresistive electrical transport pathway.

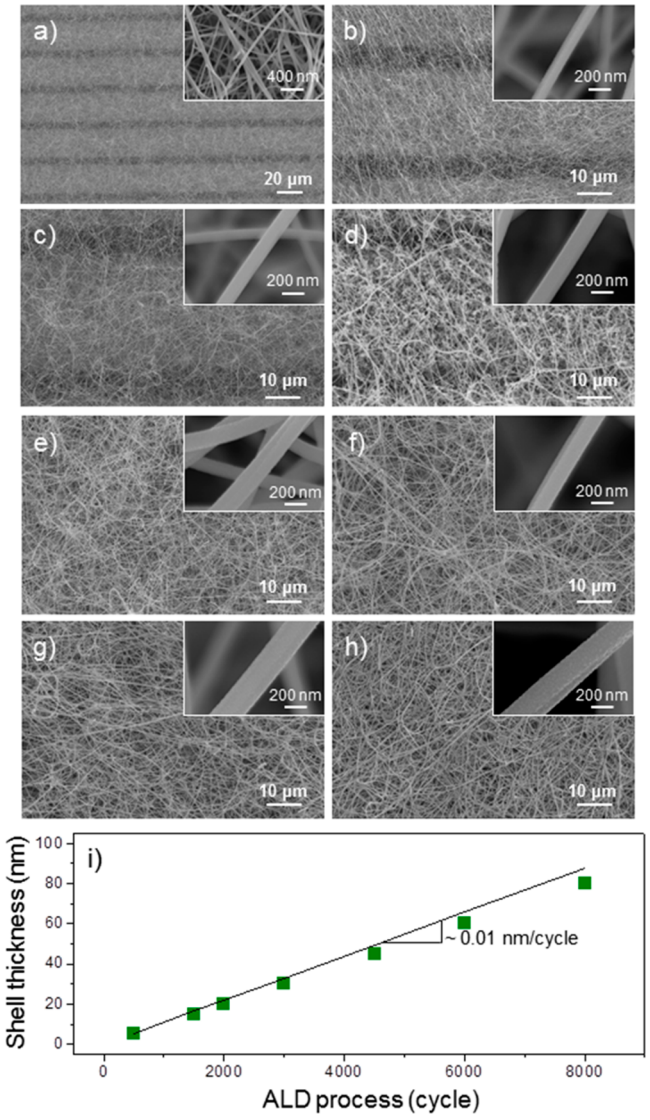

Figure 2. Typical morphologies of SnO_2−Cu_2O *n*−*p* C−S NWs with shell thicknesses of (a) 0, (b) 5, (c) 15, (d) 20 (e) 30, (f) 45, (g) 60, and (h) 80 nm. The insets are the corresponding high-magnification FE-SEM images. (i) Relationship between the shell thickness and number of ALD cycles. The slope is 0.01 nm/cycle.

DOI: 10.1021/acsami.5b03224
ACS Appl. Mater. Interfaces 2015, 7, 15351−15358

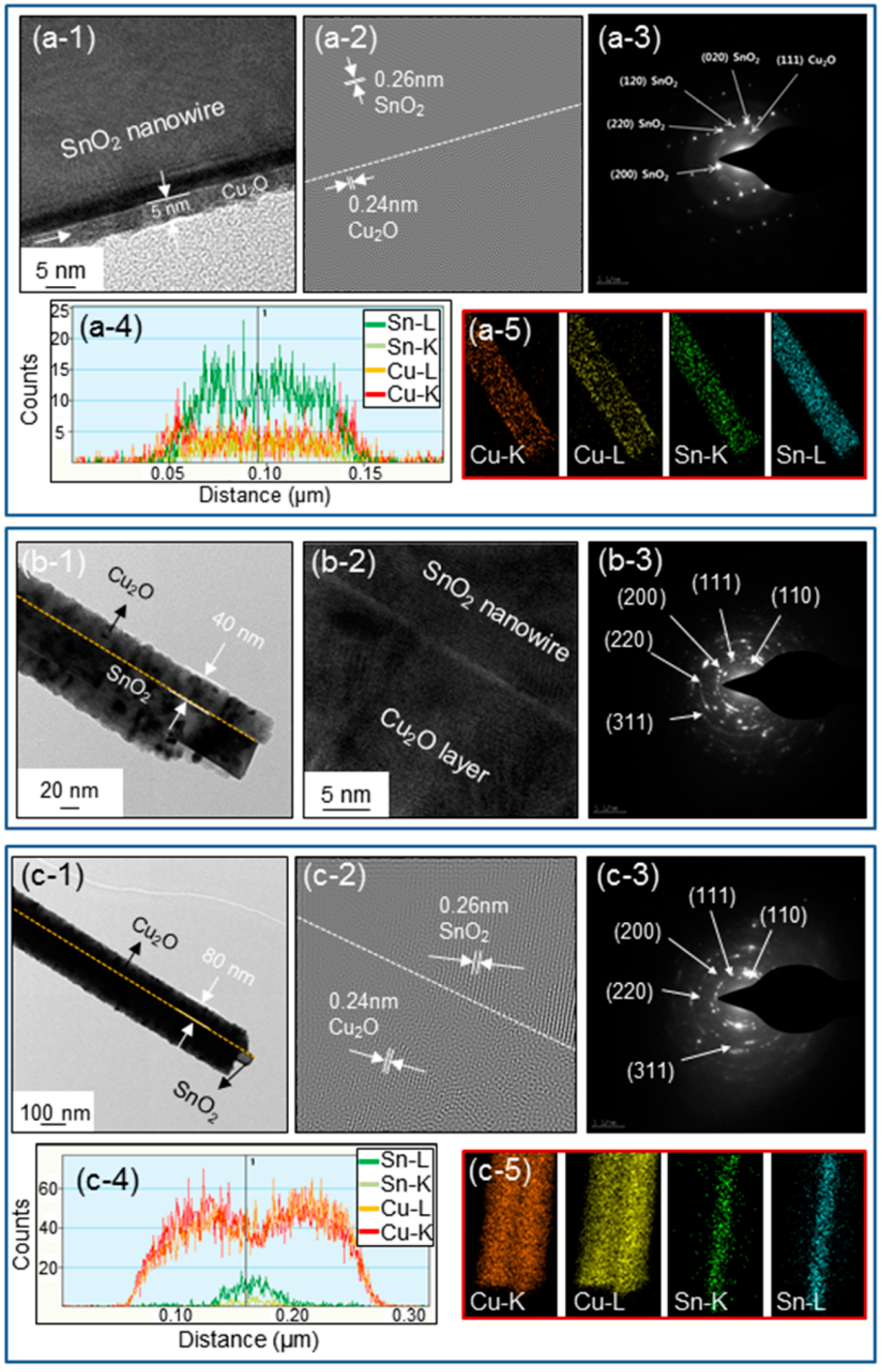

Figure 3. TEM results taken from C−S NWs with a (a) 5 nm-thick Cu_2O shell: (a-1) real high-resolution TEM image, (a-2) constructed high-resolution image, (a-3) SAED, (a-4) EDS elemental line profiles, and (a-5) elemental mappings. (b) 40 nm-thick Cu_2O shell: (b-1) bright-field TEM image, (b-2) high-resolution TEM image, and (b-3) SAED. (c) 80 nm-thick Cu_2O shell: (c-1) bright-field TEM image, (c-2) constructed high-resolution image, (c-3) SAED, (c-4) EDS elemental line profiles, and (c-5) elemental mappings.

On these networked SnO_2 NWs, Cu_2O shell layers were deposited by the ALD technique. Figures 2a−h display the SnO_2−Cu_2O C−S NWs' microstructures with a number of shell thicknesses ranging from 0 to 80 nm. The average diameter of the pristine SnO_2 NWs was ∼80 nm. The FE-SEM images clearly show that the ALD process resulted in uniform, conformal coverage of the Cu_2O shell layers on the core SnO_2 NWs even at the very small shell thickness of 5 nm. In sharp contrast to C−S nanofibers,[23] the C−S NWs do not show any evidence of nanograins, revealing high crystalline quality of NWs. It is evident that the Cu_2O shell thickness gradually increases with increasing number of ALD cycles, and that the entanglement of SnO_2 NWs is initiated at the space between the electrode pads. The shell thicknesses can be calculated from the FE-SEM images and are summarized in Figure 2i, revealing a nearly linear relationship, with a slope of 0.01 nm/cycle. Thus, a Cu_2O shell with a predetermined thickness (on the nanometer scale) can be easily synthesized on SnO_2 NWs by

DOI: 10.1021/acsami.5b03224
ACS Appl. Mater. Interfaces 2015, 7, 15351−15358

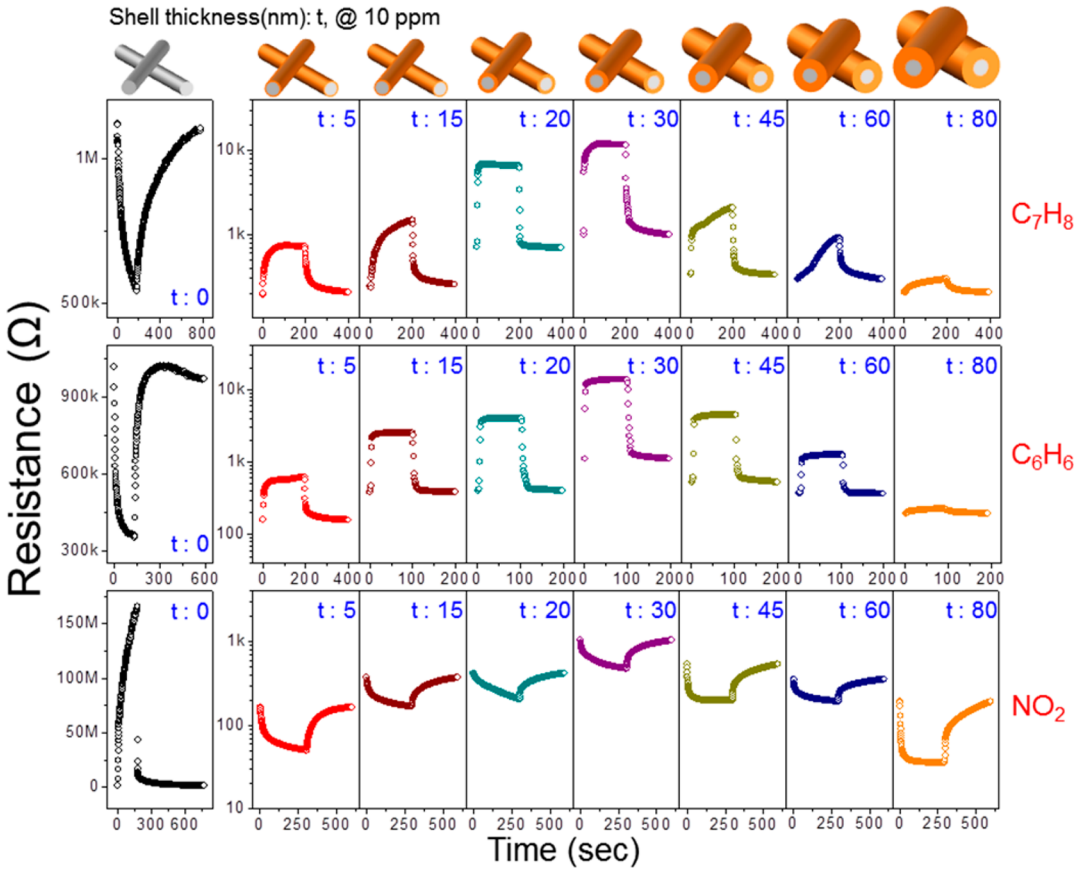

Figure 4. Resistance curves of the SnO_2−Cu_2O *n*−*p* C−S NWs with various shell thickness to 10 ppm of C_6H_6, C_7H_8, and NO_2.

changing the number of ALD cycles. In Figure S1 of the Supporting Information, the microstructures of all SnO_2−Cu_2O C−S NWs synthesized in this study with shell thicknesses ranging from 0 to 80 nm, are shown. Figures S1e-l of the Supporting Information display the magnified images showing the morphologies of SnO_2−Cu_2O C−S NWs in more detail: the surface of the NWs is smooth, without any humps or irregularities. The insets are corresponding high-magnification FE-SEM images, showing the nature of the NW entanglement in detail.

The microstructures of the SnO_2−Cu_2O C−S NWs were further investigated by TEM observations. Three typical samples were chosen for the investigation: the ones with Cu_2O shells with the minimum (5 nm), the average (40 nm), and the maximum (80 nm) thicknesses. Figure 3a shows the TEM images of C−S NWs with a 5 nm-thick Cu_2O shell. Figure 3a-1 clearly demonstrates that even the thinnest (5 nm) Cu_2O shell uniformly covers the SnO_2 NW with a very distinctive interface between the SnO_2 core and the Cu_2O shell. The high-resolution lattice image, shown in Figure 3a-2, taken from the part noted in Figure 3a-1, by using Fourier transformation of the real high resolution image highlights the sharp interface and demonstrates their single-crystal nature without any noticeable structural defects, such as dislocations or stacking faults. This directly suggests that both the ALD and vapor growth methods used for preparing the Cu_2O shells and the SnO_2 core nanowires, respectively, were well-optimized in this study. The spotty selected area electron diffraction (SAED) pattern obtained from the Cu_2O shell layer shown in Figure 3a-3 indicates the formation of well-crystallized Cu_2O. The EDS elemental line profiles and the corresponding mappings, as shown in Figures 3a-4 and 3a-5, respectively, demonstrate the localized presence of Sn in the core area, supporting the formation of a C−S structure. TEM images for the C−S NWs with a 40 nm-thick Cu_2O shell are presented in Figure 3b. The bright-field TEM image (Figure 3b-1) and the high-magnification (Figure 3b-2), TEM images both indicate the successful growth of the Cu_2O shell with uniform thickness. The SAED pattern for the sample shown in Figure 3b-3 indicates the high crystalline quality of the Cu_2O phase. The low-magnification image, the high-resolution lattice image, and the SAED pattern shown in Figures 3c-1, c-2, and c-3, respectively, demonstrate the uniform coverage of the Cu_2O shell layer, the sharp C−S interface, and excellent crystalline quality.

XRD, using a Cu Kα (1.5418 Å) source, was used to identify the crystalline phases present in the SnO_2−Cu_2O C−S NWs (Figure S2 of the Supporting Information). Both Cu_2O and SnO_2 phases are exhibited in the XRD patterns. The SnO_2 tetragonal rutile phase has lattice parameters a = 4.73 Å and c = 3.18 Å (JCPDS Card No. 88-0287), whereas the cubic phase of Cu_2O has lattice parameter a = 4.26 Å (JCPDS Card No. 65-3288), confirming the formation of SnO_2−Cu_2O C−S NWs. The intensities of the peaks corresponding to the Cu_2O phase increase with increasing shell thickness, which is due to greater amount of Cu_2O exposed to the X-ray beam, which confirms the proportional increase in the Cu_2O shell thickness with increasing number of ALD cycles.

The sensing performances of the SnO_2−Cu_2O C−S NWs with varying shell thicknesses were investigated using representative reducing gases, C_7H_8 and C_6H_6, as well as a representative oxidizing gas, NO_2. In Figure S3 of the

DOI: 10.1021/acsami.5b03224
ACS Appl. Mater. Interfaces 2015, 7, 15351−15358

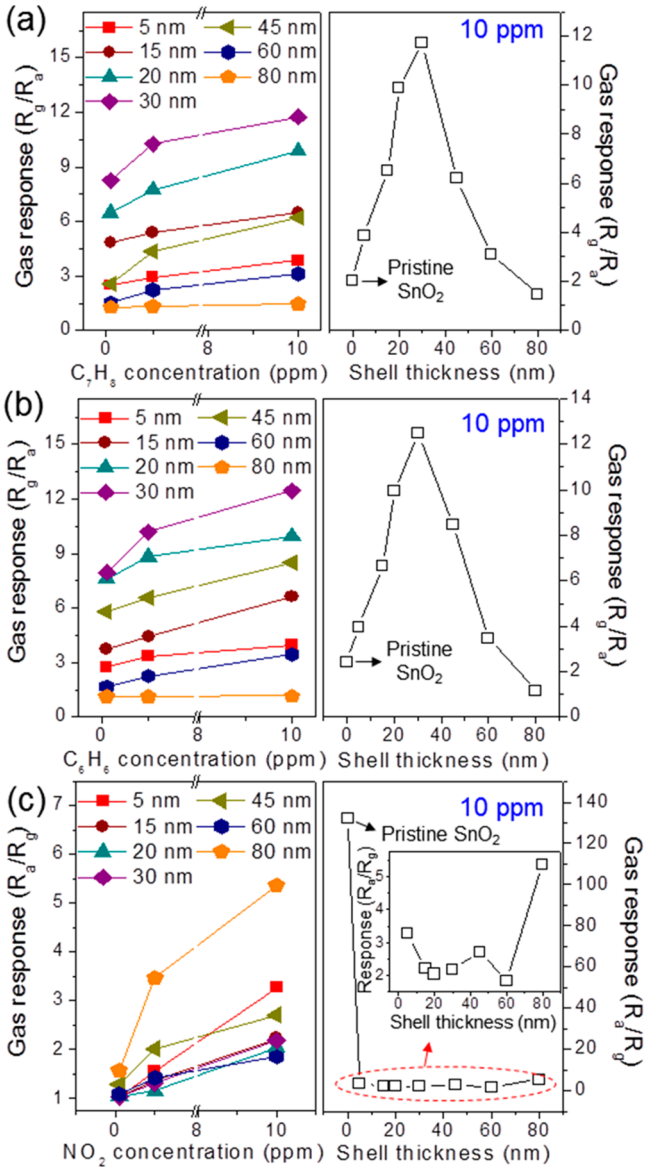

Figure 5. Summary of gas responses of the SnO_2–Cu_2O *n*–*p* C–S NWs as a function of shell thickness for: (a) C_7H_8, (b) C_6H_6, and (c) NO_2.

Supporting Information, the measured resistance curves for the above-mentioned gases are shown. For the pristine SnO_2 NWs, typical *n*-type sensing behavior is observed; the sensor resistance decreases with introduction of C_7H_8 and C_6H_6, whereas it recovers the original value when the supply of the reducing gases is stopped and air is introduced. For NO_2, the opposite resistance behavior is attained. In contrast, the SnO_2–Cu_2O C–S NWs reveal typical *p*-type sensing behavior and the gas response varies significantly with respect to shell thickness. To demonstrate the effect of Cu_2O shell thickness on the sensing properties, the resistance curves for 10 ppm of C_7H_8, C_6H_6, and NO_2 are shown in a comparative fashion in Figure 4. All the sensors are found to track changes in the gas environment: the sensor resistances increase when in the presence of reducing gases, and decrease when their supply is stopped and air is introduced. This behavior is a typical *p*-type semiconductor sensing mechanism. In ambient air, oxygen adsorbed to the surface of the Cu_2O shell extracts electrons from the Cu_2O valence band, leaving an equivalent amount of holes in the valence band, maintaining the overall resistance. The reducing gases used generally interact with the preadsorbed oxygen, creating volatile molecules, thereby returning the captured electrons back to the valence band of Cu_2O. This thins the hole-accumulation layer existing underneath the Cu_2O shell, increasing the sensor resistance. For the oxidizing gas NO_2, the resistance curves show the expected opposite behavior, due to the thickening of the hole-accumulation layer due to the additional electron capture from the Cu_2O valence band by the adsorbed NO_2, leading to a decrease in sensor resistance.[27−30] Figure 4 shows that even the C–S NWs with the thinnest shell (5 nm) exhibit *p*-type sensing behavior, demonstrating that the *p*-Cu_2O shell layer completely covered the core SnO_2 NWs, and that the *p*-Cu_2O shell governs the sensing properties of the C–S NWs. Another important feature is that the sensor response is highly dependent on the shell thickness. A detailed explanation for this feature is discussed later in this section.

As shown in Figure 5a,b, the response for the tested reducing gases, C_7H_8 and C_6H_6, of the pristine SnO_2 NW sensor is gradually enhanced by the formation of a Cu_2O shell layer on it. The C–S NW sensor with a shell thickness of 30 nm shows the best responses for the reducing gases, with any deviation from this particular shell thickness greatly deteriorating the response; responses of 11.7 and 12.5 for 10 ppm of C_7H_8 and C_6H_6, respectively. This suggests that the shell thickness needs to be optimized to obtain maximal sensing abilities for the C–S NW sensors. In contrast, as shown in Figure 5c, the presence of the Cu_2O shell layers deteriorates, rather than enhances, the sensing properties of the C–S NW sensors for the oxidizing gas NO_2. In addition, the response and recovery times of SnO_2–Cu_2O *n*–*p* C–S NWs as a function of shell thickness for 10 ppm gases were calculated, and the results are shown in Figure S4 of the Supporting Information. For the reducing gases, similar trends of response and recovery times are observed; they are shortened greatly with the optimized shell thickness. However, in sharp contrast, the response and recovery times are not associated with shell thickness for the oxidizing gas NO_2.

In a previous work[21] on SnO_2–ZnO *n*–*n* C–S NW sensors, a model for a possible sensing mechanism has been proposed based on two contributions: (1) the radial modulation of the electron-depleted shell layer and (2) the electric field smearing effect. With this model, the improvement of sensing abilities for reducing gases at a certain critical shell thickness, and the deterioration of sensing abilities for oxidizing gases, in *n*–*n* heterojunctioned C–S NW sensors were successfully explained. Although the sensing behaviors of SnO_2–Cu_2O *n*–*p* C–S NWs described here are similar to those of SnO_2–ZnO *n*–*n* C–S NWs, the sensing mechanisms operating in the two C–S NWs are different.

Figure 6 proposes the following scenario for the sensing mechanism of SnO_2–Cu_2O *n*–*p* C–S NWs. In ambient air, due to both the adsorption of oxygen onto the *p*–type Cu_2O shell and the C–S heterojunction formation, hole concentration is categorized into three regions: the hole-accumulation layer (p^+), the intrinsic hole concentration layer (p^o), and the hole-deficient layer (p^-), as described in Figure 6b. The p^+ region results from the extraction of Cu_2O valence band electrons by adsorbed oxygen species; p^o denotes the equilibrium hole concentration in Cu_2O at a particular temperature; p^- is the result of compensation by electrons in the *n*–*p* heterojunction; the red line in Figure 6b indicates the concentration profile of

DOI: 10.1021/acsami.5b03224
ACS Appl. Mater. Interfaces 2015, 7, 15351−15358

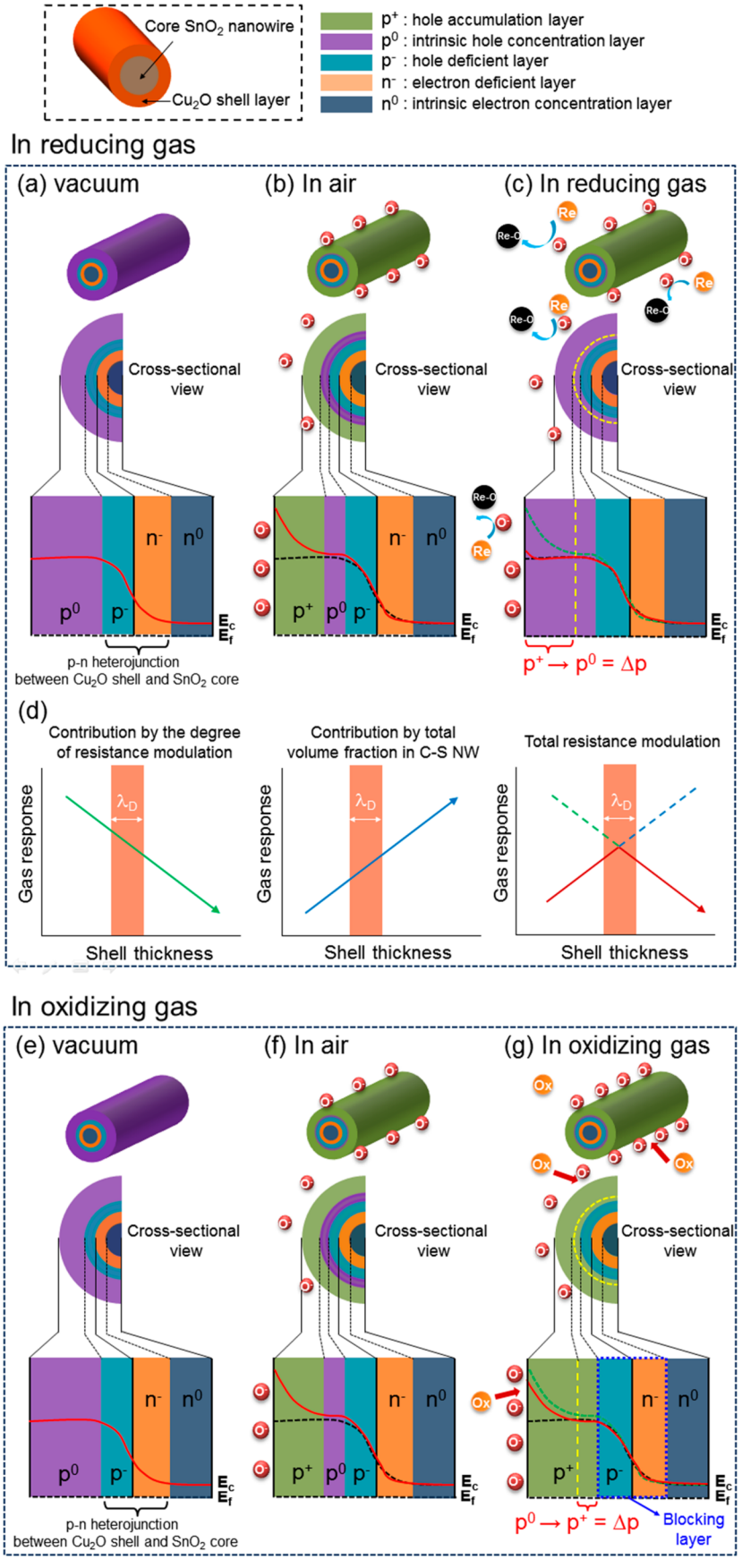

Figure 6. Conceptual description showing the sensing mechanism operating in the SnO_2–Cu_2O *n*–*p* C–S NWs for reducing gases: (a) in vacuum state, (b) in air, and (c) in reducing gases, and (d) total resistance modulation of the C–S NWs. The sensing mechanism for oxidizing gases: (e) in vacuum state, (f) in air, and (g) in oxidizing gases.

DOI: 10.1021/acsami.5b03224
ACS Appl. Mater. Interfaces 2015, 7, 15351–15358

Table 1. Comparison of the Sensing Ability of SnO_2−Cu_2O C−S NWs with Other Types of Sensing Materials

material type	gas concentration (ppm)	response (R_a/R_g)	response/recovery time (s)	temp. (°C)	ref.
SnO_2−Cu_2O C−S NWs	10 ppm of C_6H_6	12.5	4/4	300	This work
Pt nanoparticle-functionalized ZnO NWs	10	1.05	64/75	100	11
Pt-loaded Al_2O_3 catalytic filters for screen-printed WO_3	10	1.4		250	31
ZnO−TiO_2 based thick film	100	24	10/5	370	32
Ce-doped ZnO thin-film	100	3.4	15	370	33
ZnO nanorods	100	17.5		150	34
ZnO nanorods array	10	6		370	35
ZnO−Cr_2O_3 C−S NCs	5	1.06−1.68		400	36
In_2O_3−WO_3 nanofibers	100	5		275	37

holes in air ambient; the black dotted line indicates the case of vacuum state. Namely, the increase of hole concentration is created. When reducing gas molecules are supplied, the layer thins because of the evaporation of preadsorbed oxygen and liberation of captured electrons back to the valence band, eliminating holes, and consequently increasing the resistance of the p-Cu_2O shell layer; the blue line indicating the concentration profile of holes in air moves toward the red line, which indicates the decrease of hole concentration in the p shell layer. This radial modulation of the p^+ layer is the source of the total resistance modulation observed in n−p C−S NWs. It should be interesting to compare the sensing properties of pure Cu_2O NWs with those of the C−S NWs. On the basis of the above scenario, it is expected that they are inferior in comparison to the case of the C−S NWs due to the less intensified hole accumulation layer. The degree of resistance modulation originating from radial modulation of the p^+ layer varies inversely according to the shell thickness: a thinner shell may experience more pronounced resistance modulation while the thicker shell may experience less resistance modulation because the shell is in a state of partial hole-accumulation (Figure 6d). In addition to this radial modulation, we need to incorporate another contribution: the fraction of shell layers in the total volume of the n−p C−S NW. This fraction is naturally proportional to the shell thickness. Therefore, the response to a reducing gas can be depicted as the volcano-shaped curve with regard to the shell thickness. This is in good agreement with the sensing behavior observed in the n−p C−S NWs for the reducing gases, as shown in Figure 5a,b. In addition, it is of note that the two contributions are convoluted together and not possible to be separated.

According to the results shown in Figure 5c, SnO_2−Cu_2O n−p C−S NWs are not effective for the detection of the typical oxidizing gas NO_2, as the formation of Cu_2O shell layers deteriorated the NO_2-sensing performances of core NWs. As schematically shown in Figure 6e−g, the expansion of the p^+ layer is limited by the presence of the $p^-|n^-$ interface, which likely plays the role of a blocking layer to the expansion. This means that the radial modulation of the hole-accumulation layer (p^+ layer) is marginal, thereby leading to less resistance modulation for NO_2. In addition, we have compared this work with previously published results by other research groups in Table 1. The SnO_2−Cu_2O C−S NWs sensor reveals a relatively higher sensitivity in comparison to other sensing materials.

4. CONCLUSIONS

We have synthesized SnO_2−Cu_2O n−p core−shell nanowires by applying a two-step process, in which core SnO_2 nanowires were first prepared by the vapor growth technique and the Cu_2O shell layers were subsequently deposited by atomic layer deposition. Their use in chemiresistive sensors for the detection of trace amounts of gas was systematically investigated. According to the sensing measurements, the best gas-sensing performance for reducing gases was obtained at a critical p-shell thickness of 30 nm. The mutually opposite effects of the radial modulation of the hole-accumulation layer and the volume fraction contributed to the total resistance modulation with respect to the shell thickness, led to a volcano-shaped gas response behavior for reducing gases. In contrast, the presence of the p-shell deteriorated the sensing performance of core SnO_2 nanowires for a typical oxidizing gas. Blocking the expansion of the hole-accumulation layer by the p−n heterointerface is the likely source of the deterioration of NO_2-sensing performance in the n−p core−shell nanowires.

■ ASSOCIATED CONTENT

Supporting Information

Typical morphologies, XRD patterns, resistance curves, and response and recovery times of SnO_2−Cu_2O n−p C−S NWs. The Supporting Information is available free of charge on the ACS Publications website at DOI: 10.1021/acsami.5b03224.

■ AUTHOR INFORMATION

Corresponding Authors

*S. S. Kim. E-mail: sangsub@inha.ac.kr.

*S.-H. Kim. E-mail: soohyun@ynu.ac.kr.

Author Contributions

S.S.K. and S.-H..K. conceived the study, designed the experiments and prepared the manuscript. J.-H.K. and A.K. performed the experiments. All authors approved the final version of the paper.

Notes

The authors declare no competing financial interest.

■ ACKNOWLEDGMENTS

This work was supported by the Technology Innovation Program (10046707, Development of antifingerprinting coating material for touch screen window with 130° of water contact angle, 70° of oil contact angle, and more than 1500 times of antiscratch test) funded by the Ministry of Trade, Industry & Energy (MI Korea).

■ REFERENCES

(1) Kwon, O. S.; Park, S. J.; Yoon, H.; Jang, J. Highly Sensitive and Selective Chemiresistive Sensors Based on Multidimensional Polypyrrole Nanotubes. *Chem. Commun.* **2012**, *48*, 10526−10528.

(2) Penza, M.; Cassano, G.; Rossi, R.; Rizzo, A.; Signore, M. A.; Alvisi, M.; Lisi, N.; Serra, E.; Giorgi, R. Effect of Growth Catalysts on Gas Sensitivity in Carbon Nanotube Film Based Chemiresistive Sensors. *Appl. Phys. Lett.* **2007**, *90*, 103101.

DOI: 10.1021/acsami.5b03224
ACS Appl. Mater. Interfaces 2015, 7, 15351−15358

(3) Wan, Q.; Li, Q. H.; Chen, Y. J.; Wang, T. H.; He, X. L.; Li, J. P.; Lin, C. L. Fabrication and Ethanol Sensing Characteristics of ZnO Nanowire Gas Sensors. *Appl. Phys. Lett.* **2004**, *84*, 3654−3656.
(4) Sethi, S.; Nanda, R.; Chakraborty, T. Clinical Application of Volatile Organic Compound Analysis for Detecting Infectious Diseases. *Clin. Microbiol. Rev.* **2013**, *26*, 462−475.
(5) Shin, J.; Choi, S.-J.; Lee, I.; Youn, D.-Y.; Park, C. O.; Lee, J.-H.; Tuller, H. L.; Kim, I.-D. Thin-Wall Assembled SnO_2 Fibers Functionalized by Catalytic Pt Nanoparticles and Their Superior Exhaled-Breath-Sensing Properties for the Diagnosis of Diabetes. *Adv. Funct. Mater.* **2013**, *23*, 2357−2367.
(6) Kolmakov, A.; Zhang, Y.; Cheng, G.; Moskovits, M. Detection of CO and O_2 Using Tin Oxide Nanowire Sensors. *Adv. Mater.* **2003**, *15*, 997−1000.
(7) Wang, B.; Zhu, L. F.; Yang, Y. H.; Xu, N. S.; Yang, G. W. Fabrication of a SnO_2 Nanowire Gas Sensor and Sensor Performance for Hydrogen. *J. Phys. Chem. C* **2008**, *112*, 6643−6647.
(8) Gubbala, S.; Russell, H. B.; Shah, H.; Deb, B.; Jasinski, J.; Rypkema, H.; Sunkara, M. K. Surface Properties of SnO_2 Nanowires for Enhanced Performance with Dye-Sensitized Solar Cells. *Energy Environ. Sci.* **2009**, *2*, 1302−1309.
(9) Liao, L.; Zhang, Z.; Yan, B.; Zheng, Z.; Bao, Q. L.; Wu, T.; Li, C. M.; Shen, Z. X.; Zhang, J. X.; Gong, H.; Li, J. C.; Yu, T. Multifunctional CuO Nanowire Devices: p-type Field Effect Transistors and CO Gas Sensors. *Nanotechnology* **2009**, *20*, 085203.
(10) Sun, G.-J.; Choi, S.-W.; Jung, S.-H.; Katoch, A.; Kim, S. S. V-Groove SnO_2 Nanowire Sensors: Fabrication and Pt-Nanoparticle Decoration. *Nanotechnology* **2013**, *24*, 025504.
(11) Katoch, A.; Choi, S.-W.; Sun, G.-J.; Kim, S. S. Low Temperature Sensing Properties of Pt Nanoparticle-Functionalized Networked ZnO Nanowires. *J. Nanosci. Nanotechnol.* **2015**, *15*, 330−333.
(12) Yang, Z.; Guo, L.; Zu, B.; Guo, Y.; Xu, T.; Dou, X. CdS/ZnO Core/Shell Nanowire-Built Films for Enhanced Photodetecting and Optoelectronic Gas-Sensing Applications. *Adv. Opt. Mater.* **2014**, *2*, 738−745.
(13) Choi, S.-W.; Katoch, A.; Sun, G.-J.; Wu, P.; Kim, S. S. NO_2-Sensing Performance of SnO_2 Microrods by Functionalization of Ag Nanoparticles. *J. Mater. Chem. C* **2013**, *1*, 2834−2841.
(14) Zhang, Y.; Xu, J.; Xu, P.; Zhu, Y.; Chen, X.; Yu, W. Decoration of ZnO Nanowires with Pt Nanoparticles and Their Improved Gas Sensing and Photocatalytic Performance. *Nanotechnology* **2010**, *21*, 285501.
(15) Choi, S.-W.; Jung, S.-H.; Kim, S. S. Significant Enhancement of the NO_2 Sensing Capability in Networked SnO_2 Nanowires by Au Nanoparticles Synthesized Via γ-Ray Radiolysis. *J. Hazard. Mater.* **2011**, *193*, 243−248.
(16) Jang, Y.-G.; Kim, W.-S.; Kim, D.-H.; Hong, S.-H. Fabrication of Ga_2O_3/SnO_2 Core−Shell Nanowires and Their Ethanol Gas Sensing Properties. *J. Mater. Res.* **2011**, *26*, 2322−2327.
(17) Li, X.; Li, X.; Chen, N.; Li, X.; Zhang, J.; Yu, J.; Wang, J.; Tang, Z. CuO-In_2O_3 Core-Shell Nanowire Based Chemical Gas Sensors. *J. Nanomater.* **2014**, *2014*, 1−7.
(18) Kim, S. S.; Na, H. G.; Choi, S.-W.; Kwak, D. S.; Kim, H. W. Decoration of Pd Nanoparticles on ZnO-Branched Nanowires and Their Application to Chemical Sensors. *Microelectron. Eng.* **2013**, *105*, 1−7.
(19) Zhu, C. L.; Chen, Y. J.; Wang, R. X.; Wang, L. J.; Cao, M. S.; Shi, X. L. Synthesis and Enhanced Ethanol Sensing Properties of α-Fe_2O_3/ZnO Heteronanostructures. *Sens. Actuators, B* **2009**, *140*, 185−189.
(20) Shuai, X. M.; Shen, W. Z. A Facile Chemical Conversion Synthesis of ZnO/ZnS Core/Shell Nanorods and Diverse Metal Sulfide Nanotubes. *J. Phys. Chem. C* **2011**, *115*, 6415−6422.
(21) Choi, S.-W.; Katoch, A.; Sun, G.-J.; Kim, J.-H.; Kim, S.-H.; Kim, S. S. Dual Functional Sensing Mechanism in SnO_2−ZnO Core−Shell Nanowires. *ACS Appl. Mater. Interfaces* **2014**, *6*, 8281−8287.
(22) Katoch, A.; Kim, J.-H.; Kim, S. S. TiO_2/ZnO Inner/Outer Double-Layer Hollow Fibers for Improved Detection of Reducing Gases. *ACS Appl. Mater. Interfaces* **2014**, *6*, 21494−21499.
(23) Katoch, A.; Choi, S.-W.; Sun, G.-J.; Kim, H. W.; Kim, S. S. Mechanism and Prominent Enhancement of Sensing Ability to Reducing Gases in p/n Core−Shell Nanofibers. *Nanotechnology* **2014**, *25*, 175501.
(24) Park, J. Y.; Choi, S.-W.; Kim, S. S. Junction-Tuned SnO_2 Nanowires and Their Sensing Properties. *J. Phys. Chem. C* **2011**, *115*, 12774−12781.
(25) Choi, S.-W.; Katoch, A.; Kim, J.-H.; Kim, S. S. Prominent Reducing Gas-Sensing Performances of n-SnO_2 Nanowires by Local Creation of p−n Heterojunctions by Functionalization with p-Cr_2O_3 Nanoparticles. *ACS Appl. Mater. Interfaces* **2014**, *6*, 17723−17729.
(26) Choi, S.-W.; Katoch, A.; Kim, J.-H.; Kim, S. S. Striking Sensing Improvement of n-type Oxide Nanowires by Electronic Sensitization Based on Work Function Difference. *J. Mater. Chem. C* **2015**, *3*, 1521−1527.
(27) Varghese, O. K.; Kichambre, P. D.; Gong, D.; Ong, K. G.; Dickey, E. C.; Grimes, C. A. Gas Sensing Characteristics of Multi-Wall Carbon Nanotubes. *Sens. Actuators, B* **2001**, *81*, 32−41.
(28) Hoa, N. D.; Quy, N. V.; Tuan, M. A.; Hieu, N. V. Facile Synthesis of p-type Semiconducting Cupric Oxide Nanowires and Their Gas-Sensing Properties. *Phys. E* **2009**, *42*, 146−149.
(29) Liao, L.; Zhang, Z.; Yan, B.; Zheng, Z.; Bao, Q. L.; Wu, T.; Li, C. M.; Shen, Z. X.; Zhang, J. X.; Gong, H.; Li, J. C.; Yu, T. Multifunctional CuO Nanowire Devices: p-type Field Effect Transistors and CO Gas Sensors. *Nanotechnology* **2009**, *20*, 085203.
(30) Wang, C.; Fu, X. Q.; Xue, X. Y.; Wang, Y. G.; Wang, T. H. Surface Accumulation Conduction Controlled Sensing Characteristic of p-type CuO Nanorods Induced by Oxygen Adsorption. *Nanotechnology* **2007**, *18*, 145506.
(31) Hubalek, J.; Malysz, K.; Prasek, J.; Vilanova, X.; Ivanov, P.; Llobet, E.; Brezmes, J.; Correig, X.; Sverak, Z. Pt-Loaded Al_2O_3 Catalytic Filters for Screen-Printed WO_3 Sensors Highly Selective to Benzene. *Sens. Actuators, B* **2004**, *101*, 277−283.
(32) Zhu, B. L.; Xie, C. S.; Wang, W. Y.; Huang, K. J.; Hu, J. H. Improvement in Gas Sensitivity of ZnO Thick Film to Volatile Organic Compounds (VOCs) by Adding TiO_2. *Mater. Lett.* **2004**, *58*, 624−629.
(33) Ge, C.; Xie, C.; Cai, S. Preparation and Gas-Sensing Properties of Ce-Doped ZnO Thin-Film Sensors by Dip-Coating. *Mater. Sci. Eng., B* **2007**, *137*, 53−58.
(34) Lv, Y.; Guo, L.; Xu, H.; Chu, X. Gas-Sensing Properties of Well-Crystalline ZnO Nanorods Grown by a Simple Route. *Phys. E* **2007**, *36*, 102−105.
(35) Tian, S.; Yang, F.; Zeng, D.; Xie, C. Solution-Processed Gas Sensors Based on ZnO Nanorods Array with an Exposed (0001) Facet for Enhanced Gas-Sensing Properties. *J. Phys. Chem. C* **2012**, *116*, 10586−10591.
(36) Woo, H.-S.; Na, C. W.; Kim, I.-D.; Lee, J.-H. Highly Sensitive and Selective Trimethylamine Sensor Using One-Dimensional ZnO−Cr2O3 Hetero-Nanostructures. *Nanotechnology* **2012**, *23*, 245501.
(37) Feng, C.; Li, X.; Ma, J.; Sun, Y.; Wang, C.; Sun, P.; Zheng, J.; Lu, G. Facile Synthesis and Gas Sensing Properties of In_2O_3−WO_3 Heterojunction Nanofibers. *Sens. Actuators, B* **2015**, *209*, 622−629.

DOI: 10.1021/acsami.5b03224
ACS Appl. Mater. Interfaces 2015, 7, 15351−15358